Viscoplastic Flow Through a Sudden Expansion

Article *in* AIChE Journal · October 2001

DOI: 10.1002/aic.690471004

3 authors, including:

Pascal Jay
Université Grenoble Alpes
43 PUBLICATIONS **708** CITATIONS

SEE PROFILE

Viscoplastic Fluid Flow Through a Sudden Axisymmetric Expansion

Pascal Jay, Albert Magnin, and Jean Michel Piau
Laboratoire de Rhéologie, University of Grenoble (UJF, INPG) and CNRS (UMR 5520),
38041 Grenoble Cedex 9, France

Numerical experiments were carried out for yield-stress fluid flows through a 1:4 sudden axisymmetric expansion using the Herschel-Bulkley and Bingham models with a two-viscosity approximation. The influence of shear thinning, inertia and yield-stress values on the structure of the flow and on pressure and head losses was studied. The detailed structure of flow in the expansion shows an initial vortex. The yield stress generates two toroidal rigid dead zones, one located in the corner of the expansion and one located close to the stagnation point that appears between the vortex and the downstream flow. Inertia and yield stress act in opposite ways. When inertia increases, the vortex increases in size and the rigid dead zone decreases. Conversely, when yield stress increases, the vortex decreases in size and the rigid dead zone increases. Shear thinning reduces the dimensions of both vortices and dead zones. Pressure loss increases with yield stress. In addition, the numerical results are consistently compared with experimental ones.

Introduction

Pastes, slurries, and food products are soft materials that display viscoplasticity and can be modeled using a Herschel-Bulkley constitutive equation or its restriction in a Bingham model (Prager, 1961). In both models, a yield stress value is introduced, and no flow conditions prevail at low stress levels. For stress levels higher than the yield-stress value, flow displays Newtonian viscosity with a Bingham model, whereas shear thinning or shear thickening occurs with a Herschel-Bulkley model. Recent publications by Nguyen and Boger (1992), Wilson (1993), Piau (1996, 1998), and Barnes (1999) have drawn attention to key aspects of this field of research and given some fundamental results.

This article describes a numerical study of the flow of these fluids through an axisymmetric expansion. Few authors have worked on this subject. Aribert and Doustens (1981) proposed a numerical variational method using a kinematically admissible velocity field applied to a Bingham model. Using this method, it was possible to determine the pressure drop vs. the Bingham number for a sudden change of section and for different expansion ratios in plane and axisymmetric geometries. Their experiments showed good agreement with their numerical results. Scott et al. (1988) described a finite-element method for calculating flows of Bingham and Casson models through abrupt planar and axisymmetric expansions. They studied vortex intensity vs. Reynolds number and Bingham number for expansion ratios of 1:2 and 1:3. They showed that the extent and strength of recirculation are lower for viscoplastic models than for Newtonian models. Vradis and Ötügen (1997) used a finite difference technique and studied the internally separating flow of a Bingham model for a ratio of 2, Reynolds numbers from 2 to 100, and yield-stress numbers from 0 to 10. They showed the pronounced effect that these variables have on recirculating flow and particularly the decrease in reattachment length and strength of the recirculating flow as the yield numbers increase. Recently, Burgos and Alexandrou (1999) used a finite-element formulation to study the flow of a Herschel-Bulkley model through a 1:2 sudden three-dimensional square expansion. They studied the influence of the Reynolds number, Bingham number, and

Correspondence concerning this article should be addressed to P. Jay.

power-law index on the structure of the flow. It was shown that the extent of the core regions decreases with the Reynolds number and increases with both the Bingham number and the power-law index.

In all articles concerning axisymmetric geometries, the influence of the governing parameters is studied systematically, but this is not true of the detailed structure of flow in the corner and in the central zone. The presence of a central moving rigid zone is not shown. Moreover, no comparison is made with experimental results. So the aim of this article is to show the change in structure and particularly in unyielded zones (rigid dead zones in the corner and central rigid moving zones) with the flow parameters, yield stress number, Reynolds number, and shear thinning index. The pressure loss and the head loss are also calculated as a function of these parameters.

The flow of a viscoplastic fluid through a 1:4 sudden axisymmetric expansion is studied with a finite-element code. After a presentation of the numerical problem and experimental setup, the change in flow in the corner and central zones of the pipe is shown as a function of the shear thinning index, Herschel-Bulkley number and Reynolds number. The influence of these parameters on pressure and head losses is also demonstrated. Comparisons with experimental results are made in the last section.

Numerical Modeling

The flow of an incompressible fluid in isothermal conditions with no slip at the wall is considered. The governing equations are therefore those of mass and momentum conservation. The finite-element program "Polyflow" developed by FLUENT Inc. is used.

Adaptation of Bingham and Herschel-Bulkley models

For a generalized Newtonian model

$$\boldsymbol{T} = 2\eta(\dot{\gamma})\boldsymbol{D}, \tag{1}$$

where $\boldsymbol{T}$ is the extra-stress tensor, η the viscosity, $\boldsymbol{D}$ the rate of deformation tensor, and $\dot{\gamma}$ the rate of deformation intensity defined as a second invariant of $\boldsymbol{D}$

$$\dot{\gamma} = \sqrt{2\boldsymbol{D}:\boldsymbol{D}}\,. \tag{2}$$

Using τ_0 to denote the yield stress, K the consistency factor, T_2 the second invariant of $\boldsymbol{T}$ defined by an equation similar to Eq. 2 for a Herschel-Bulkley model, then

$$\begin{aligned} \boldsymbol{T} &= 2\left(\frac{\tau_0}{\dot{\gamma}} + K(\dot{\gamma})^{(n-1)}\right)\boldsymbol{D} \quad \text{if} \quad T_2 > \tau_0^2 \\ \boldsymbol{D} &= 0 \qquad\qquad\qquad\qquad\quad \text{if} \quad T_2 \le \tau_0^2, \end{aligned} \tag{3}$$

where n is the shear thinning index; for a Bingham model, n is equal to 1.

Using the velocity and pressure parameters as main variables leads to a singularity. Viscosity becomes infinite when shear rate vanishes. It is possible to overcome this difficulty by introducing an exponential part in the expression of the viscosity, as proposed by Papanastasiou (1987). Abdali et al. (1992), Mitsoulis et al. (1993), Isayev and Huang (1993) (with a slightly modified version), Loest et al. (1994), Burgos and Alexandrou (1999) used the same model in their studies of a viscoplastic medium. It is also possible to introduce a "two-viscosity model" as proposed by Lipscomb and Denn (1984) and used by O'Donovan and Tanner (1984), Wilson (1993), and Vradis and Ötügen (1997). Under a critical shear rate $\dot{\gamma}_c$, the viscosity is constant and equal to the viscosity obtained at $\dot{\gamma} = \dot{\gamma}_c$ by the Bingham and Herschel-Bulkley models. Above $\dot{\gamma}_c$, the viscosity is given by the model

$$\begin{aligned} \boldsymbol{T} &= 2\left(\frac{\tau_0}{\dot{\gamma}} + K(\dot{\gamma})^{(n-1)}\right)\boldsymbol{D} \quad \text{if} \quad \dot{\gamma} > \dot{\gamma}_c \\ T &= 2\left(\frac{\tau_0}{\dot{\gamma}_c} + K(\dot{\gamma}_c)^{(n-1)}\right)\boldsymbol{D} \quad \text{if} \quad \dot{\gamma} \le \dot{\gamma}_c. \end{aligned} \tag{4}$$

Thus, the model is continuous. This "two-viscosity model" is used in this study. The optimum $\dot{\gamma}_c$ will be determined in the subsection on characterization of unyielded zones.

Burgos et al. (1999) discussed the ability of a Herschel-Bulkley model transformed into a two-viscosity model or Papanastasiou model to determine the structure of the yield surface in the case of shear flow in a wedge between two rigid walls. In comparison with the analytical solution, they showed that the Papanastasiou model predicts the yield surface well while the two-viscosity model predicts the stress field away from $\tau = \tau_0$ well. In this article (subsection titled "Characterization of Unyielded Zones") it is shown that with an optimum choice of critical shear rate (used in the two-viscosity model), it is also possible to achieve a relatively good determination of the yield surface.

Nondimensionalization

Dimensionless equations are formed by scaling velocities with the average velocity U_2 in the small tube, distances with the radius R_2 of the same tube and the viscosity with η_0 defined by

$$\eta_0 = K\left(\frac{U_2}{R_2}\right)^{(n-1)}. \tag{5}$$

The dimensionless flow rate is then equal to π.

The three dimensionless numbers appearing in the momentum equation are:

- The Herschel-Bulkley number

$$Hb = \frac{\tau_0}{K\left(\frac{U_2}{R_2}\right)^n}. \tag{6}$$

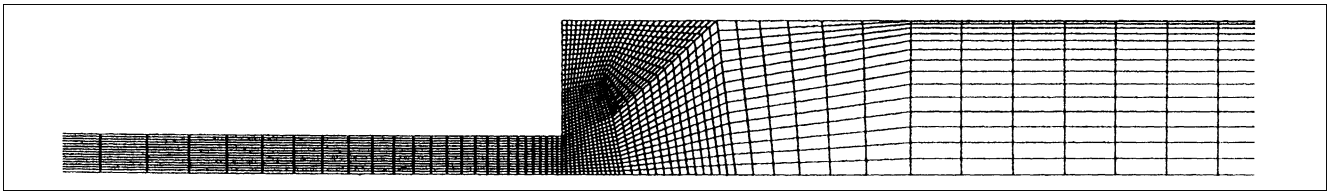

Figure 1. Mesh used throughout this study: 7,123 nodes; 1,728 elements.

- The Reynolds number

$$\mathrm{Re} = \frac{\rho R_2 U_2}{K\left(\frac{U_2}{R_2}\right)^{(n-1)}}, \quad \rho \text{ is the density of the fluid,} \quad (7)$$

- The shear thinning index n.

Boundary conditions and mesh

The geometry studied is a 1:4 sudden axisymmetric expansion. Flow at the inlet (length L_2, radius R_2) and the outlet (length L_1, radius R_1) is assumed to be fully developed ($L_2/R_2 = 20$, $L_1/R_2 = 25$). At the solid walls, the velocity satisfies no-slip conditions.

The influence of the mesh on the results has been studied systematically. In order to obtain accurate results for the rigid dead zone and vortex shape, the mesh is highly refined in the corner of the expansion (Figure 1). In this part, the results are independent of the mesh. The rest of the mesh corresponding to the main flow has larger elements in order to maintain a reasonable CPU time. The established radius (R_y) of the rigid central zone and the different lengths H (Figure 2) are also independent of the mesh. The mesh finally chosen for this study (Figure 1) has 7123 nodes and 1728 elements. Recommencing with the data from the case where ($Hb = 0.1$, $Re = 0$, $n = 0.37$), the CPU time needed to obtain results corresponding to the parameters $Hb = 1$, $Re = 0$, and $n = 0.37$ is about 427 min on an HP 715/33 computer.

Vortex characterization

The corner vortex is studied using the stream function ψ. A value of zero is imposed at the wall. So the limit between the main flow and the vortex is obtained by tracking the isoline $\psi = 0$.

Characterization of unyielded zones

Determination of critical shear rate. With the purely viscous approximation used in this work, the limit of the unyielded zones is not defined by $\dot{\gamma} = 0$ but by $\dot{\gamma} < \dot{\gamma}_c$. So the choice of $\dot{\gamma}_c$ is extremely important. To obtain accurate unyielded zones, the value of $\dot{\gamma}_c$ must be as small as possible. On the other hand, this value must be large enough to ensure a reasonable CPU time. O'Donovan and Tanner (1984) propose a criterion on the $\dot{\gamma}_c$ independence of results. For the two-viscosity model, this criterion can be used to calculate the permissible value of $\dot{\gamma}_c$

$$\dot{\gamma}_c \leq \left(\frac{\tau_0}{999K}\right)^{1/n} \quad (8)$$

For the experimental cases studied in this article: $\tau_0 = 25.7$ Pa, $n = 0.37$, $K = 1.5$ Pa·s^n. Hence: $\dot{\gamma}_c \leq 1.68 \times 10^{-5}\,\mathrm{s}^{-1}$. For the numerical cases, different values can be found with this criterion, between $\dot{\gamma}_c = 10^{-2}$ (for $Hb = 200$, $n = 0.37$) and $\dot{\gamma}_c = 10^{-9}$ (for $Hb = 1$, $n = 0.37$).

Figure 2 shows the unyielded zones obtained for $\dot{\gamma}_c = 10^{-2}$ and $\dot{\gamma}_c = 10^{-9}$, for $Hb = 1$ and $n = 0.37$. It can be observed that these zones are totally different: for $\dot{\gamma}_c = 10^{-9}$, the downstream rigid moving zone is pushed away from the corner and it is much smaller than in the case of $\dot{\gamma}_c = 10^{-2}$. The same effect can be observed for the upstream rigid moving zone. The rigid dead zone in the corner is also smaller.

Two methods were chosen to quantify these changes with $\dot{\gamma}_c$. The first consists in measuring the rigid moving zone directly, and the second in calculating the size of this zone by evaluating the wall shear stress:

- Using the first way, different characteristic lengths of the unyielded regions are measured directly on the figures (Figure 2) and adimensionalized by the entrance radius R_2. $(R_y/R_2)_\eta$, $(H/R_2)_\eta$, and $(H_1/R_2)_\eta$ were obtained using this way.

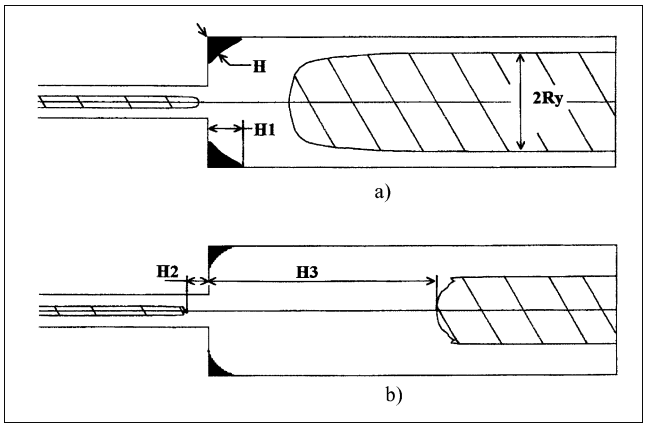

Figure 2. Influence of $\dot{\gamma}_c$ on the unyielded zones.

(a) $\dot{\gamma}_c = 10^{-2}$; (b) $\dot{\gamma}_c = 10^{-9}$; $Hb = 1$, $n = 0.37$, Reynolds number negligible. Rigid dead zones in black; rigid moving zones hatched.

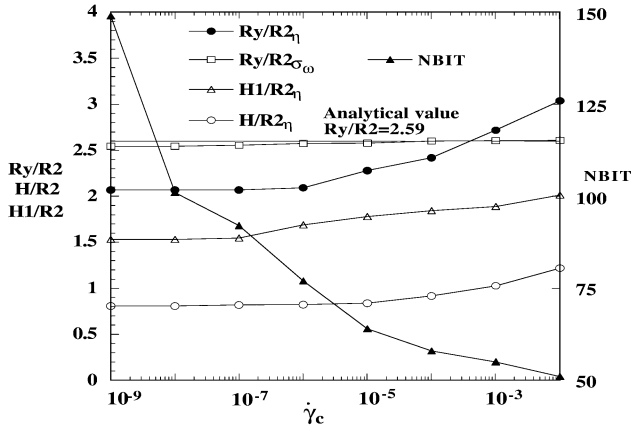

Figure 3. Change in R_y/R_2, H/R_2, H_1/R_2, the number of iterations NBIT vs. $\dot{\gamma}_c$: $Hb = 1$, $n = 0.37$, Reynolds number negligible.

• It is also possible to calculate the diameter of the rigid moving zone by a second method. For a pipe of length L and radius R, the wall shear stress can be calculated with the pressure loss ΔP

$$\sigma_\omega = R\frac{\Delta P}{2L}. \tag{9}$$

As $a = (\sigma_0/\sigma_\omega) = R_y/R$, the radius R_y can be calculated by numerical determination of the pressure loss. Here, $(R_y/R_2)_{\sigma_\omega}$ was obtained by this method, using the same parameters as previously.

The change in these lengths with $\dot{\gamma}_c$ is given in Figure 3. Moreover, the number of iterations NBIT to obtain convergence was also calculated as a function of $\dot{\gamma}_c$. Convergence is achieved when the norm of the change in solution vector between successive iterations is less than 10^{-5}.

First, it may be noticed that the geometric values (H, H_1, R_y) decrease with $\dot{\gamma}_c$, but very slowly up to $\dot{\gamma}_c = 10^{-7}$. The value obtained with the wall shear stress is almost constant whatever the critical shear rate. The values obtained for $\dot{\gamma}_c = 10^{-5}$ differ between 12% (for the worst case, H_1) and 1% (H) from those obtained for $\dot{\gamma}_c = 10^{-7}$. On the other hand, the number of iterations increases drastically with $\dot{\gamma}_c$ above $\dot{\gamma}_c = 10^{-5}$. So this value of the critical shear rate seems to be a good compromise between accuracy and calculation time.

Comparison with analytical values. For the axisymmetric geometry of this study, it is possible to calculate the analytical solution of the velocity field, but also the radius of the rigid moving zone in both the entrance and exit tubes for fully developed flow.

For a capillary of radius R, the flow rate Q can be expressed by the relation

$$Q = \frac{1}{\sigma_\omega^2}\int_{\tau_0}^{\sigma_\omega}\sigma^2 f(\sigma)\,d\sigma, \tag{10}$$

with, for a Herschel-Bulkley model

$$f(\sigma) = \left(\frac{\sigma - \tau_0}{K}\right)^{1/n}. \tag{11}$$

By integration, it can be obtained with $a = (\tau_0/\sigma_\omega)$ and $m = (1/n)$

$$\frac{Q}{\pi R^3} = \frac{(1-a)^{m+1}}{m+3}\left(\frac{\tau_0}{aK}\right)^m\left[1 + \frac{2a}{m+2} + \frac{2a^2}{(m+1)(m+2)}\right]. \tag{12}$$

This relation can be expressed with dimensionless variables

$$Q_{a\,\mathrm{dim}}\frac{R_2^3}{\pi R^3} = \frac{(1-a)^{m+1}}{m+3}\left(\frac{Hb}{a}\right)^m\left[1 + \frac{2a}{m+2} + \frac{2a^2}{(m+1)(m+2)}\right]. \tag{13}$$

As $Q_{a\,\mathrm{dim}} = \pi$, this relation becomes

$$\frac{R_2^3}{R^3} = \frac{(1-a)^{m+1}}{m+3}\left(\frac{Hb}{a}\right)^m\left[1 + \frac{2a}{m+2} + \frac{2a^2}{(m+1)(m+2)}\right]. \tag{14}$$

It is also possible to express the variable a with R_y, the radius of the rigid moving zone

$$a = \frac{\tau_0}{\sigma_\omega} = \frac{R_y}{R}. \tag{15}$$

So, for a given Hb, it is possible by solving Eq. 14 to obtain the value of a, and thus the radius R_y.

Solving Eq. 12 gives a value of 2.59 in the previous case (Figure 3) for R_y/R_2. So, using the wall shear stress, evaluation gives a very good approximation of R_y/R_2 ($(R_y/R_2)_{\sigma_\omega}$ between 2.609 and 2.544), almost regardless of the critical shear rate value. The method using unyielded zones also gives the analytical solution. This is obtained for a value of $\dot{\gamma}_c$ situated between 10^{-3} and 10^{-4}. For $\dot{\gamma}_c = 10^{-5}$, $(R_y/R_2)_{\sigma_\omega}$ is equal to 2.578 and $(R_y/R_2)_\eta$ is equal to 2.28, which corresponds to relative errors of 0.5 and 12% respectively. So the value $\dot{\gamma}_c = 10^{-5}$ still seems to be a good compromise.

The value $\dot{\gamma}_c = 10^{-5}$ thus gives a good approximation of the size of the unyielded zones both where the flow is fully devel-

oped (for R_y) and where it is not (for H and H_1). Moreover the corresponding CPU time is reasonable. This value was therefore chosen for all the calculations in this work.

Pressure and head-loss calculations

Pressure losses were characterized by the equivalent entrance length, defined by

$$L_{\text{eq}} = \frac{\Delta P_S}{2\sigma_{\omega_2}}, \tag{16}$$

where ΔP_s represents the additional pressure loss due to the singularity, calculated in the following way

$$\Delta P_s = \Delta P - \Delta P_1 - \Delta P_2, \tag{17}$$

where ΔP is the total pressure drop; ΔP_i is the pressure drop in fully developed Poiseuille flow in a tube of length L_i and radius R_i; σ_{ω_2} is the wall shear stress in fully developed Poiseuille flow in a tube of radius R_2.

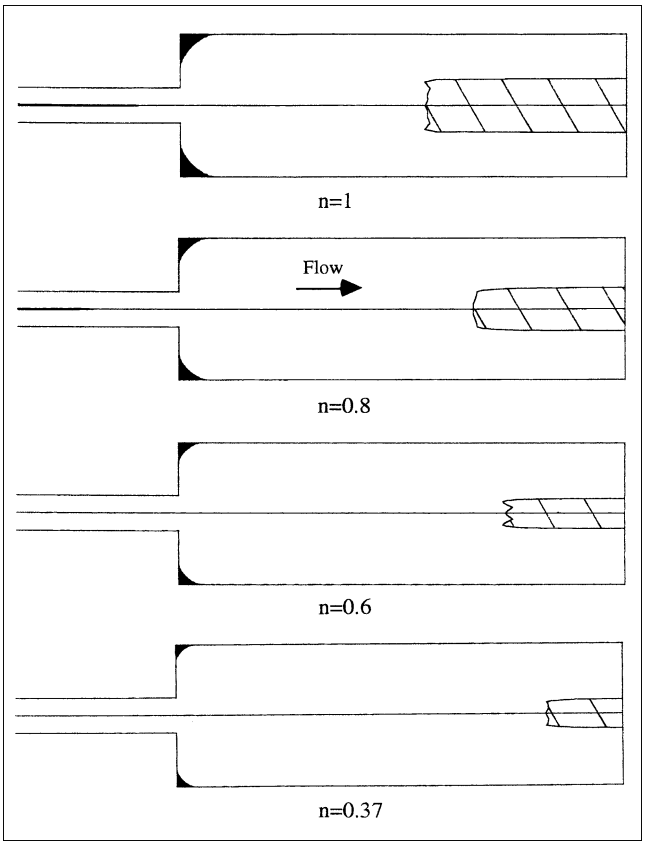

Figure 4. Influence of the shear thinning index on yielded surfaces.

$Hb = 10^{-1}$; Reynolds number negligible; rigid dead zones in black; rigid moving zones hatched.

The head loss is also characterized by the mean of an equivalent length (see the Appendix) defined by

$$L'_{\text{eq}} = \frac{\Delta E_s}{2\sigma_{\omega_2}} \tag{18}$$

where ΔE_s is the loss of energy due to the expansion.

Experimental Setup

Our group previously investigated viscoplastic fluid flows through axisymmetric expansions experimentally (Belhadri et al., 1994, Magnin and Piau, 1992, Kouamela, 1991). The experimental setup is described by Belhadri et al. (1994). This is designed visualizing the kinematic field. Original processes and technological solutions have been used to overcome the problems occurring with plasticity. The polymer used, Carbopol 940, is a shear thinning transparent yield-stress fluid. It has been rheometrically characterized and it has been shown that it follows the Herschel-Bulkley law (Magnin and Piau, 1990).

Results

Morphology of flows

The flow of a yield-stress fluid has a distinctive structure. For a given geometry, this structure changes with the shear thinning index, yield stress, and inertia. Fully developed flow in a tube consists of a peripheral viscous flow and a central rigid moving zone. In the corner, there is a vortex and/or a rigid dead zone.

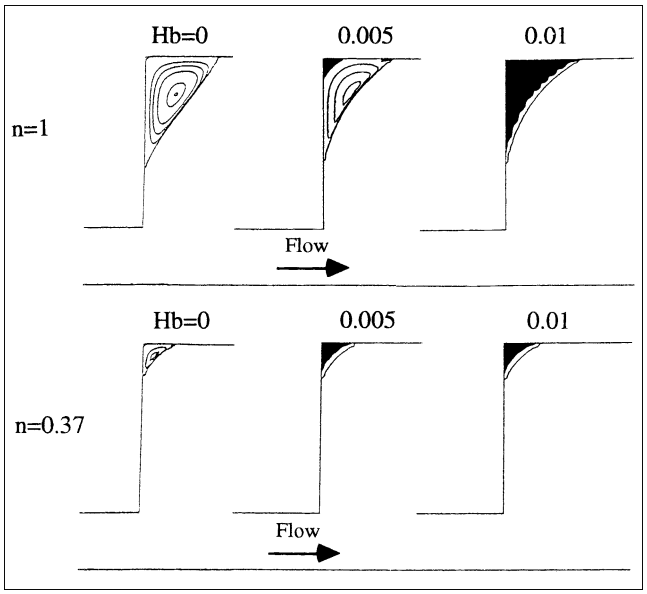

Figure 5. Influence of the shear thinning index on flow in the corner: Reynolds number negligible.

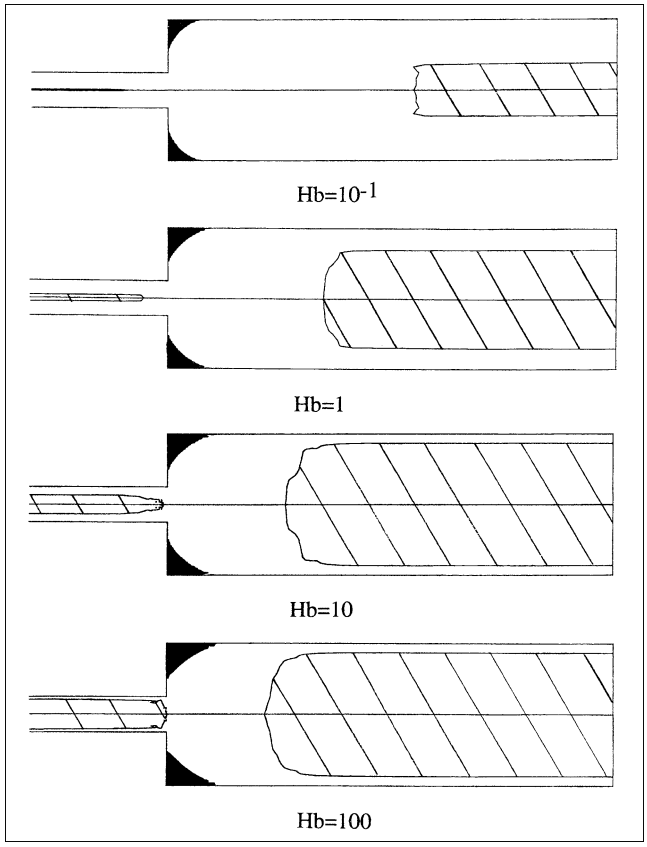

Figure 6. Influence of the Herschel-Bulkley number on yielded surfaces.

$n = 1$, Reynolds number negligible.

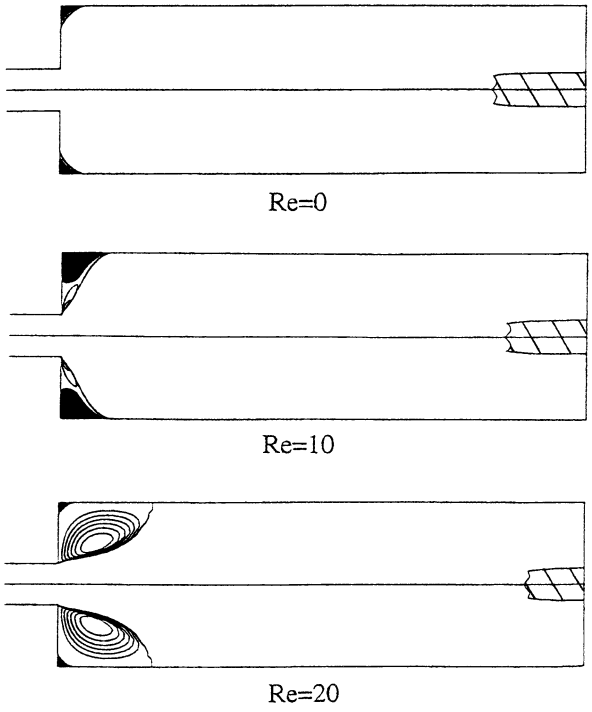

Figure 7. Evolution of the structure of the flow in relation to *Re* number.

$Hb = 10^{-1}$, $n = 0.37$.

The aim of this section is to define the structural changes in the divergent flow, depending on the values of n and Hb, first in cases of flows with negligible inertia (Figures 4 to 6), and secondly for flows with inertia (Figures 7 to 9) for various values of the Reynolds number. The calculations were performed for $n = 1$ (Bingham model) and for $n = 0.37$, which fits with the experimental data. The Reynolds numbers and Herschel-Bulkley numbers were varied from 0 to 50 and from 0 to 200, respectively. In these figures, the rigid dead zones are drawn in black and the rigid moving zones are hatched. The continuous line represents the limit of the main flow ($\psi = 0$).

1. Flows without inertia

(a) Influence of the Shear Thinning Index. It is interesting to analyze the change in morphology as a function of the shear thinning index. Figure 4 shows this for $Hb = 0.1$. When n decreases, the radius of the downstream rigid moving zone decreases drastically. It is practically halved from $n = 1$ to $n = 0.37$. This zone is also pushed down the flow. When n decreases, the rigid dead zone in the corner also decreases significantly; for $n = 0.37$, it almost disappears. For the upstream central rigid moving zone, as the value of Hb is very small, its radius is very small. Therefore, this zone does not appear very clearly in the figures. It is possible to calculate it analytically, as shown previously in the case of the downstream flow. For $Hb = 0.1$ and $n = 0.37$, the radius of the upstream rigid moving zone may be 0.049 times the radius of the entry tube. This zone therefore does not appear on the

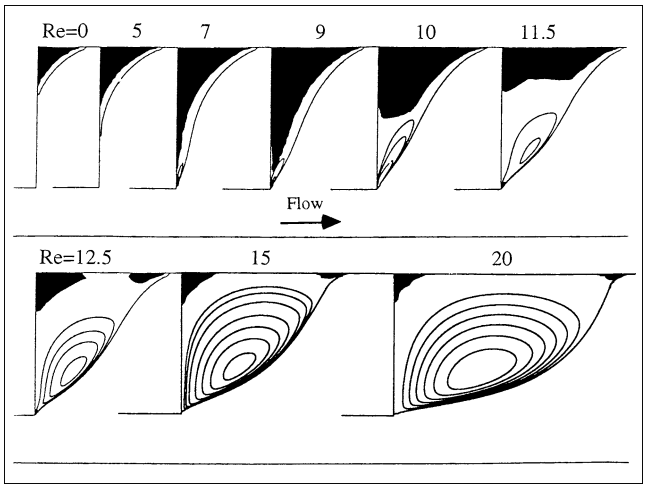

Figure 8. Change in flow structure in relation to *Re* number.

$Hb = 10^{-1}$. $n = 0.37$: zoom on the corner.

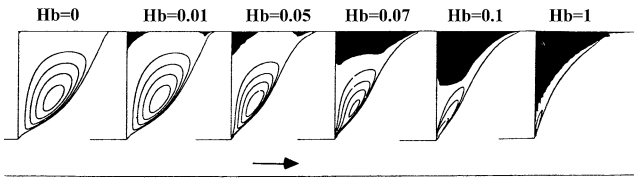

Figure 9. Change in flow structure in relation to *Hb* number.

Re = 10, *n* = 0.37: zoom on the corner.

figures, but it must exist. Nevertheless, for $n = 1$ and $n = 0.8$ it is possible to see them and to note that when n decreases, this zone is pushed back.

For a greater Hb ($Hb > 10$), it also has been shown that the effects of shear thinning are much less important, and there are few differences between the cases in which $n = 0.37$ and $n = 1$. The influence of the shear thinning index on the morphology of the flow in the corner is shown in greater detail in Figure 5. For $Hb = 0$, it may be noted that shear thinning reduces the upstream vortex, as shown by Kim et al. (1983) for a contraction flow. For $n = 1$, the Newtonian vortex fills the entire corner. On the other hand, for $n = 0.37$, the vortex is pushed completely into the corner and takes up very little room there. It is also interesting to note that the intensity of the vortex found in this work is very close to that proposed by Kim et al. (1983). They found a vortex intensity of 1.8×10^{-3} for a flow rate of 1, that is, a value of 5.625×10^{-3} for a flow rate of π. In this work, a value of 5.5×10^{-3} was found. The shape and size of the vortex are also very close.

For $Hb = 0.005$, two unyielded zones can be found in the case of the Bingham model, corresponding to low stress zones: a rigid dead zone in the corner and a very small one at the stagnation point between the vortex and the main flow (this will be studied in more detail in a later section). For a shear thinning fluid ($n = 0.37$), there is just a rigid dead zone in the corner. This is slightly larger than in the case of the Bingham model.

For $Hb = 0.01$ in both cases, there is just a rigid dead zone in the corner. But now, in contrast to previously, the rigid dead zone for the shear thinning fluid is very much smaller than in the Bingham model. When there is no vortex, shear thinning therefore tends to reduce the size of the rigid dead zone.

(b) Influence of the Herschel-Bulkley Number

With the previous figure (Figure 5), it is also possible to examine the influence of the Herschel-Bulkley number on the structure of the flow. In the corner, for $n = 0.37$, the small vortex obtained for $Hb = 0$ is immediately replaced by the corner rigid dead zone as soon as a yield stress is introduced ($Hb = 0.005$). The rigid dead zone therefore increases very slightly in size for $Hb = 0.01$. For $n = 1$ and $Hb = 0.005$, as seen previously, the size of the vortex decreases and two rigid dead zones appear: a rigid dead zone in the corner and a very small one at the break point between the vortex and the main flow. With a higher Hb ($Hb = 0.01$), the vortex vanishes, and the rigid dead zones in the corner and the stagnation point merge into a single large one. This takes up almost all the room occupied by the Newtonian vortex ($Hb = 0$).

Figure 6 obtained for $n = 1$ and a negligible Reynolds number shows the influence of the Hb number on the unyielded zones. As previously, it can be seen, that the Herschel-Bulkley number increases the size of the rigid dead zone. For $Hb = 0.1$ the rigid dead zone occupies little room in the corner. In contrast, for $Hb = 100$, it occupies a very large space. It may also be noted that the Hb number drastically increases the size of the rigid central moving zone both upstream and downstream. For example, for $Hb = 0.1$, the upstream rigid zone in the figure is very small. On the other hand, for $Hb = 100$, it takes up practically all the room in the entry tube. With the same value of Hb, the rigid moving zone also occupies a large part of the downstream tube. It may also be noted that the length from the exit tube to the beginning of the rigid moving zones changes little between $Hb = 10$ and $Hb = 100$. The same remark could be made in relation to the radius. It is possible to calculate them analytically, as seen previously: between $Hb = 10$ and $Hb = 100$ the radius has to change by just 4%. It is therefore natural not to observe differences in the figure for these two cases.

2. Flows with inertia

Influence of the Reynolds number. In the case of a Herschel-Bulkley model ($n = 0.37$, $Hb = 0.1$), when the Reynolds number increases (Figure 7) the downstream rigid moving zone is pushed away. As a vortex is created in the corner, this zone seems to be almost pushed back by it. The radius of the rigid moving zone is always unchanged for the different Re values.

In the corner (Figure 8), when the Re number is negligible, there is only a small rigid dead zone. As inertia increases, the rigid dead zone increases in size until it reaches the exit border of the small tube at an Re number of about 7. Then a vortex appears. In contrast to the Newtonian model, it grows not from the corner of the expansion but from the exit border of the small tube. It cannot extend from the corner because the rigid dead zone opposes its growth. The vortex begins to replace the rigid dead zone as Re exceeds 9. Just before $Re = 12.5$, the rigid dead zone is cut into two parts, one in the corner and one at the stagnation point between the vortex and the main flow. This rigid dead zone cut into two parts has never been noted previously. It was also obtained experimentally (see the last section). Generally, as shown by Macagno and Hung (1967), but for Newtonian flows, the reattachment length increases with increasing inertia.

Influence of the Herschel-Bulkley Number. In this section, $Re = 10$ and n = 0.37. In the corner (Figure 9), there is only a vortex created by inertia when $Hb = 0$. When yield stress effect increases, two rigid dead zones grow, one from the corner of the expansion and one from the break point of the vortex to the wall. As the Hb number continues to grow, the rigid dead zones coalesce and the vortex is replaced by a single rigid dead zone ($Hb = 7 \times 10^{-2}$) until the vortex disappears at the exit border of the small tube ($Hb = 1$). As mentioned by Vradis and Ötügen (1997), but for a downstream-to-upstream diameter ratio of two and a Bingham model, the

reattachment length can be seen to decrease with increasing yield numbers.

For the rigid moving zones, the same evolution as in Figure 6 (for a Reynolds number negligible) has been observed: for $Hb = 10^{-1}$, the rigid moving zones are very small and for $Hb = 100$, practically all the volume of the upstream and the downstream tubes is occupied by these two zones.

These figures thus show that the change in flow morphology is strongly dependent on the three dimensionless numbers. With regard to the rigid dead zone, *Re* and *Hb* act in opposite ways when there is a vortex. Inertia tends to reduce the rigid dead zone, and yield stress tends to extend it. The increase in shear thinning index tends to reduce it slightly. When there is no vortex or a very small one, *Re* and *Hb* act in the same way by increasing the size of the rigid dead zone. This zone is also enlarged with the shear thinning index. In the case of the central rigid moving zones, *Re* has no influence on their fully developed flow radius. On the other hand, it pushes them away, upstream in the case of the entrance tube and downstream in the case of the exit tube. The radius of these zones increases drastically with the *Hb* number.

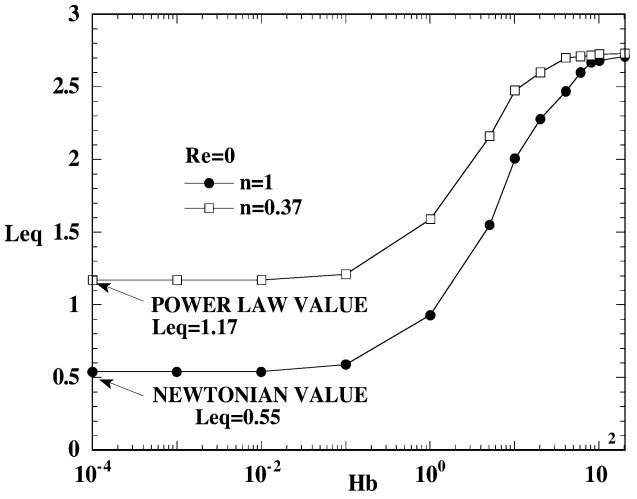

Figure 11. Influence of the Herschel-Bulkley number on pressure loss.

Reynolds number negligible.

Vortex map

From a practical point of view, for example, to design an experimental setup or an industrial process, it is interesting to know whether there is a vortex or not when depending on *Hb* or *Re* values. To solve this problem, a map of vortex formation was prepared for the present experimental case corresponding to $n = 0.37$. This map (Figure 10) was drawn after a systematic analysis of the morphology of the flow for *Hb* numbers between 10^{-2} and 10 and Re numbers from 1 to 50. With this map it is possible to determine whether or not there is a vortex in the corner for a given (*Hb*, *Re*) pair. It is not easy to determine the exact moment when the vortex appears, because it is necessary to scan a very wide range of Re numbers for each *Hb* number. So an area of doubt is indicated instead of an exact value. From this figure, it can be observed that the limit of occurrence of the vortex increases with the yield stress number. For $Hb = 10^{-2}$, the flow displays a vortex above a Reynolds number of 10, while with $Hb = 10$, the Reynolds number must be greater than 50.

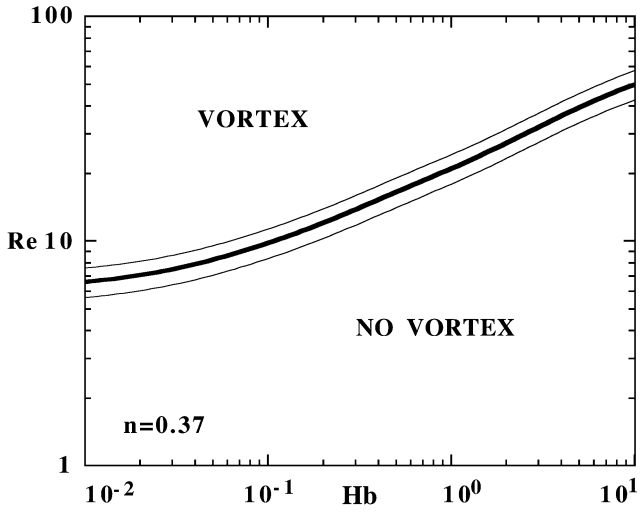

Figure 10. Map of vortex occurrence.

$n = 0.37$.

Pressure and head losses

As previously, it is also interesting from the technological point of view to estimate the pressure and head losses due to the singularity. Two cases are examined: first when the inertia is negligible and second when it is greater.

Case of Negligible Inertia. Figure 11 illustrates the influence of the yield stress on the equivalent entrance length, which characterizes pressure losses, as mentioned earlier. The cases corresponding to the Bingham and Herschel-Bulkley models are examined. For $Hb = 0$, the Newtonian and power-law values of 0.55 and 1.17, respectively, are found. These values are very close to those proposed by Kim et al. (1983) and Crochet et al. (1984). The first found 0.58 and 1.11, and the second found only between 0.548 and 0.555 for the Newtonian case, depending on the mesh refinement.

For *Hb* numbers smaller than 10^{-1}, L_{eq} is almost constant for the two curves. In this case, viscous effects play a the major role. On the other hand, from this value onwards, yield effects become increasingly important and pressure loss increases drastically with the yield-stress number. For $Hb = 100$, the two curves nearly merge. The shear thinning effect then becomes negligible and the L_{eq} depends only on the *Hb* number. The values increase slightly up to $L_{eq} = 2.68$ for $n = 1$ and $L_{eq} = 2.72$ for $n = 0.37$ when $Hb = 200$.

Influence of inertia. Figure 12 shows the influence of *Re* for different values of *Hb*. For *Re* numbers smaller than 1, that is, when inertia effects are weak, pressure loss is independent of *Re* and only dependent on *Hb*. For larger *Re* numbers, L_{eq} decreases with increasing *Re* and becomes a gain instead of a loss of pressure. This is due to the slowing down of the flow due to the advent of the vortex in the corner of the expansion (Figure 8). As the kinetic energy de-

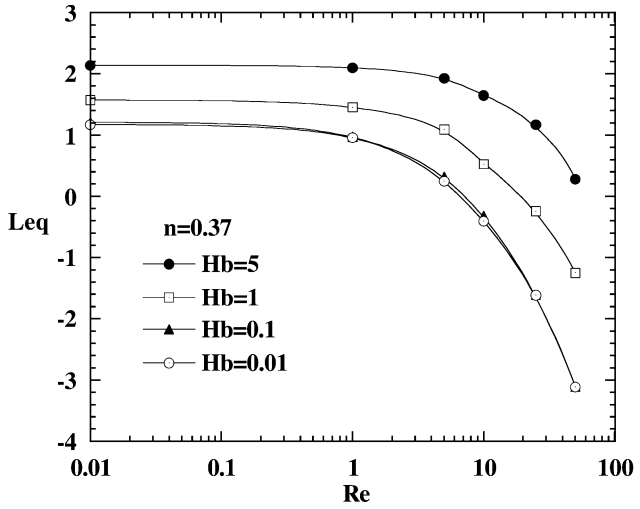

Figure 12. Influence of the Reynolds number on pressure loss.

$n = 0.37$.

creases, the pressure must increase to ensure energy conservation. For all Reynolds numbers, it can also be found that pressure loss increases with *Hb*.

Figure 13, which is easier to use in defining a setup, displays head loss for the same condition as Figure 12. With small Reynolds numbers, head loss again appears to be independent of Re, but it increases with *Hb*. In this case, as inertia effects are weak, the variations in kinetic energy are negligible. For the largest Reynolds numbers, the opposite is true: L′eq decreases as *Hb* increases. In fact, for high Reynolds numbers (Figure 8), vortices are the main cause of energy loss. But the yield stress, as shown by Figure 9, tends to delay its occurrence. The increase in *Hb* therefore allows a reduction in L'_{eq} for a given Reynolds number.

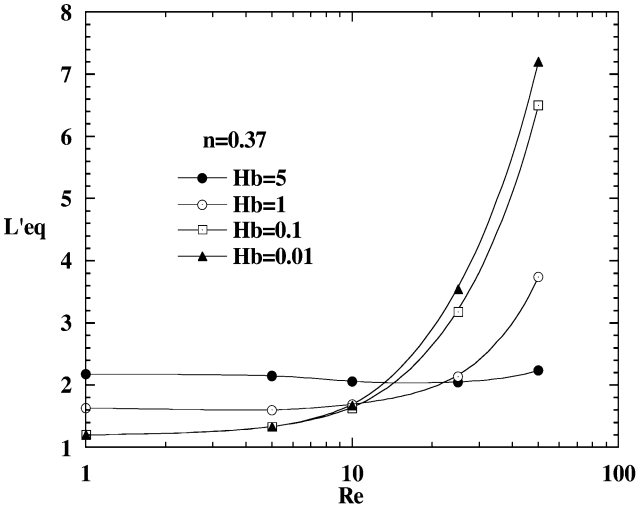

Figure 13. Influence of the Reynolds number on head loss.

n = 0.37

Comparison with experimental observations

Experimental investigations of yield-stress fluid flows through axisymmetric expansions are currently being carried

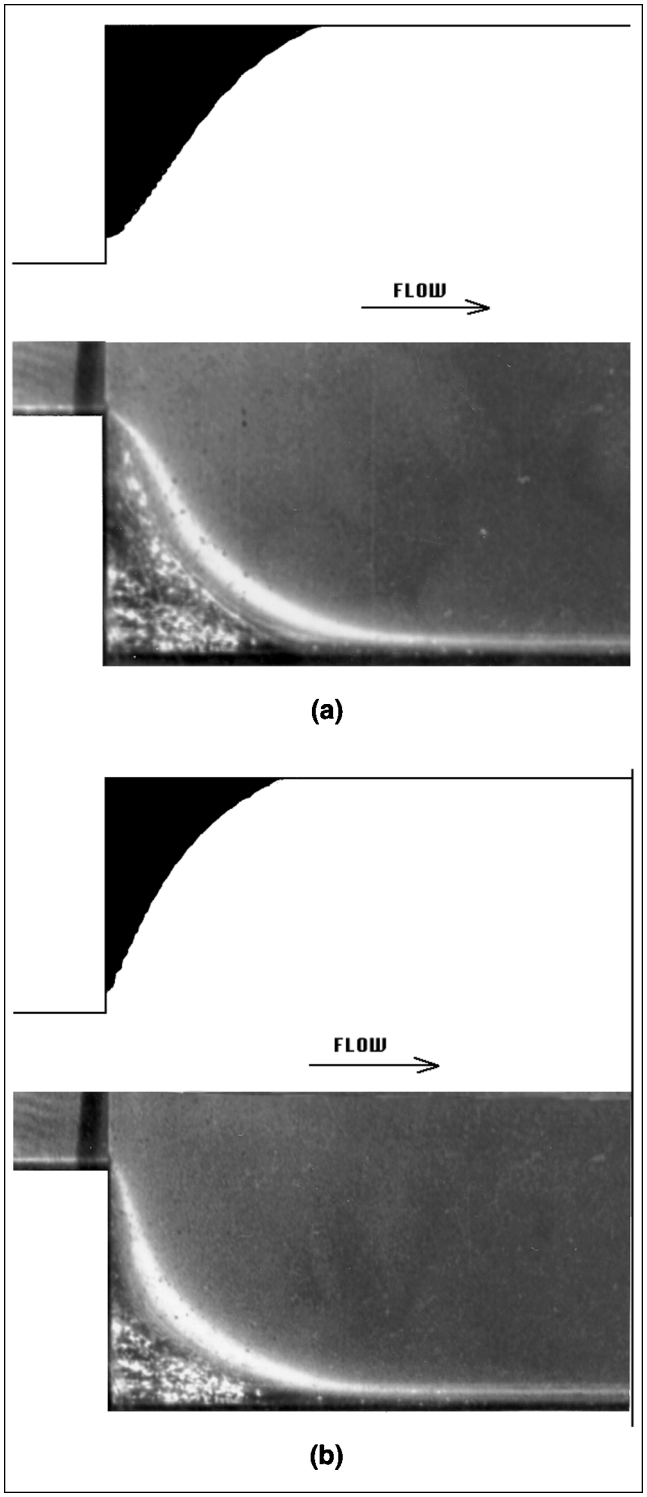

Figure 14. Comparison of numerical and experimental results.

(a) $Re = 10.34$, $Hb = 0.267$, $n = 0.37$, $\tau_0 = 25.7$ Pa, $K = 1.5$ Pa·s^n; (b) $Re = 13.67$, $Hb = 0.252$, $n = 0.37$, $\tau_0 = 25.7$ Pa, $K = 1.5$ Pa·s^n.

out in our laboratory. Carbopol 940 flowing through transparent dies is used to display the vortex and rigid dead zones for different *Hb* and Reynolds numbers. It is thus possible to compare experimental and numerical results. Figures 14 and 15 show four different cases. Yield-stress effects dominate for the flow represented on Figure 14a ($Re = 10.34$ and $Hb = 0.267$) whereas inertia effect dominates in the case of figure 15b ($Re = 25.34$ and $Hb = 0.221$). The configuration obtained when neither inertia nor yield stress is preponderant is plotted in Figure 15a ($Re = 19.3$ and $Hb = 0.234$). Qualitatively, general agreement can be observed between the numerical simulation and the experimental results in terms of both the size of the rigid dead zone and the vortex. Numerically, the effects of inertia and yield stress are the same as those observed experimentally. When the *Hb* number decreases the size of the rigid dead zone (Figure 14a, 14b) decreases. For larger *Re* numbers, inertia prevails, and so the vortex grows and the rigid dead zone decreases (Figures 15a and 15b). As mentioned in the numerical section, the vortex begins to extend from the exit corner of the small tube. The rigid dead zone is finally cut into two parts (Figure 15b), one situated in the corner and the other at the stagnation point between the vortex and the main flow, as described previously. The shape and size of the rigid dead zones are in good agreement, quantitatively speaking. Nevertheless, the calculated vortex core is slightly displaced toward the exit of the small tube.

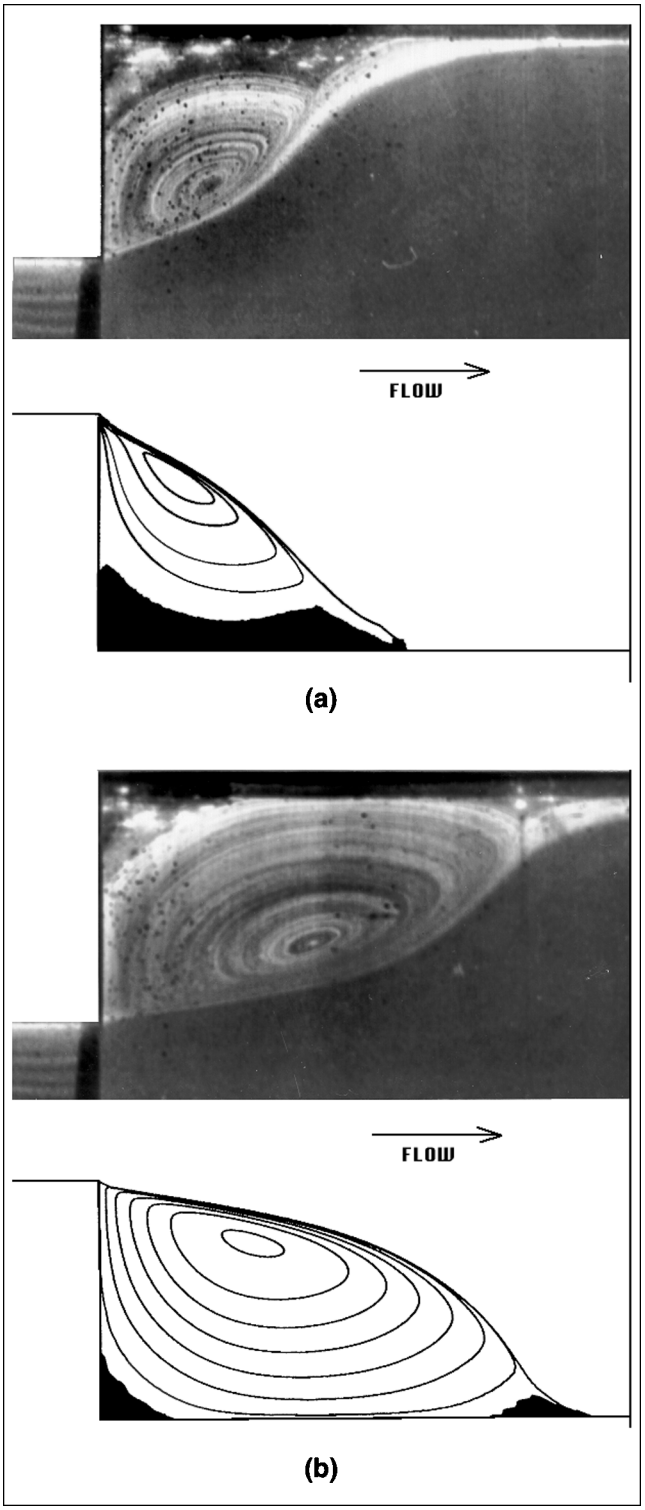

Figure 15. Comparison of numerical and experimental results.

(a) $Re = 19.3$. $Hb = 0.234$. $n = 0.37$, $\tau_o = 25.7$ Pa, $K = 1.5$ Pa·s^n; (b) $Re = 25.34$, $Hb = 0.221$. $n = 0.37$, $\tau_0 = 25.7$ Pa, $K = 1.5$ Pa·s^n.

Conclusions

Numerical experiments were performed concerning the flow of viscoplastic Bingham and Herschel-Bulkley models through a sudden axisymmetric expansion. The detailed structure of the flow was studied. In the corner of the expansion, a vortex and a rigid dead zone can be found, as well as another rigid dead zone at the break point between the vortex and the main flow. There is also a rigid moving zone in the central part of the flow in both the upstream and downstream pipes.

The influence of the governing parameters, that is, the Reynolds number, Herschel-Bulkley number, and shear thinning index on this structure is identified. It is shown that, when there is an initial vortex, the Reynolds number and the Herschel-Bulkley number have opposite effects on the size of the rigid dead zone: when the Reynolds number increases, the vortex increases and the size of the rigid dead zone size decreases. When the Herschel-Bulkley number increases, the opposite occurs. The shear thinning index tends to reduce it slightly.

When there is no vortex or only a very small one, *Re* and *Hb* act in the same way: they extend the rigid dead zone. This zone increases also with the shear thinning index. The Reynolds number does not modify the radius of the central rigid moving zone with fully developed flow, but rather shifts its position. In contrast, its size depends considerably on the *Hb* number. For the highest *Hb*, practically all the volume of the upstream and downstream pipes is occupied by the rigid moving zone. The shear thinning index tends to increase its size, especially for small *Hb* numbers.

For technological reasons, a map was prepared showing vortex occurrence in relation to the Reynolds and yield-stress numbers. With this map, it is possible to determine the presence of any vortex in a 1:4 expansion for a given yield stress fluid. Pressure and head losses also depend on *Hb* and *Re*.

Pressure loss increases with *Hb* for all Reynolds numbers. On the other hand, with regard to energy loss, L'_{eq} increases with *Hb* for small *Re*, but because of the reduction in upstream vortex decreases with *Hb* for large *Re*.

The results obtained from experiments with the Herschel-Bulkley model flows through axisymmetric expansions performed in the Laboratoire de Rhéologie for different *Re* and *Hb* numbers were compared with numerical results. In particular, comparisons were made concerning the vortex and rigid dead zone. Qualitatively speaking, the same mechanisms were obtained as those found numerically. In particular, an unyielded zone located at the stagnation point between the vortex and the main flow was found both numerically and experimentally. Vortex extension from the exit border of the small tube was also determined in both ways. Quantitatively, general agreement can be observed.

Notation

$\boldsymbol{D}$ = rate-of-strain tensor
g = gravity
Hb = Herschel-Bulkley number
K = fluid consistency
L_{eq} = equivalent length for pressure
L'_{eq} = equivalent length for head loss
L_1 = length of exit section
L_2 = length of entry section
n = power-law index
$NBIT$ = number of iterations
P = pressure
Q = flow rate
Q_{adim} = dimensionless flow rate
R = radius
Re = Reynolds number
R_y = radius of the downstream moving rigid zone
$\boldsymbol{T}$ = extra stress tensor
U = average velocity

Greek letters

$\dot{\gamma}$ = shear rate
$\dot{\gamma}_c$ = critical shear rate
ΔP_s = variation in pressure due to a sudden expansion
ΔE_s = mechanical energy loss due to a sudden expansion
η = viscosity
ρ = density of fluid
σ = shear stress
τ_0 = yield stress
σ_ω = wall shear stress
ψ = stream function

Subscripts

1 = exit tube
2 = entry tube
ω = at the wall
max = maximum value

Literature Cited

Abdali, S. S., E. Mitsoulis, and N. C. Markatos, "Entry and Exit Flows of Bingham Fluids," *J. Rheol.*, **36**, 389 (1992).

Aribert, J. R., and A. Doustens, "Etude Théorique et Expérimentale, d'Écoulements Binghamiens dans un Élargissement Brusque de Section," *J. Mec.,* **20**, 591 (1981).

Barnes, H. A., "The Yield Stress—A Review or $\pi\alpha\nu\tau\alpha$ $\rho\epsilon$—Everything Flows?," *J. of Non-Newtonian Fluid Mech.*, **81**, 133 (1999).

Belhadri, M., A. Magnin, and J. M. Piau, "Ecoulements en charge de Fluides à seuil dans les geometries complexes," *Actes du 8*^{éme} *Colloque TIFAN*, Toulouse, France (1994).

Burgos, G. R., A. N. Alexandrou, and V. Entov, "On the Determination of Yield Surfaces in Herschel-Bulkley Fluids," *J. Rheol.,* **43**, 463 (1999).

Burgos, G. R., and A. N. Alexandrou, "Flow Development of Herschel-Bulkley Fluids in a Sudden Three Dimensional Square Expansion," *J. Rheol.*, **43**, 485 (1999).

Crochet, M. J., A. R. Davies, and K. Walters, "Numerical Simulation of Non-Newtonian Flow," Elsevier, Amsterdam (1984).

Isayev, A. I., and Y. H. Huang, "Two-Dimensional Planar Flow of a Viscoelastic Plastic Medium," *Rheol. Acta*, **32**, 181 (1993).

Kim-E M. E., R. A. Brown, and R. C. Armstrong, "The Roles of Inertia and Shear Thinning in Flow of Inelastic Liquid Through an Axisymmetric Contraction," *J. Non-Newtonian Fluid Mech.*, **13**, 41 (1983).

Kouamela, D., "Etude Expérimentale des Écoulements en Charge de Fluides à Seuil," PhD Thesis, Institut National Polytechnique de Grenoble INPG, Grenoble, France (1991).

Lipscomb, G. G., and M. M. Denn, "Flow of Bingham Fluids in Complex Geometries," *J. Non-Newtonian Fluid Mech.*, **14**, 337 (1984).

Loest, H., R. Lipp, and E. Mitsoulis, "Numerical Flow Simulation of Viscoplastic Slurries and Design Criteria for a Tape Casting Unit," *J. Amer. Ceram. Soc.*, **77**, 254 (1994).

Macagno, E. O., and T.-K. Hung, "Computional and Experimental Study of a Captive Annular Eddy," *J. Fluid Mech.*, **28**, 43 (1967).

Magnin, A., and J. M. Piau, "Cone Plate Rheometry of a Yield Stress Fluid. Measurement of an Aqueous Gel," *J. Non-Newtonian Fluid Mech.*, **36**, 85 (1990).

Magnin, A., and J. M Piau, "Flow of Yield Stress Fluids Through a Sudden Change of Section," *Theoretical and Applied Rheology*, Vol. 1. P. Moldenaers and R. Keunings, eds., Elsevier, Amsterdam, p. 195 (1992) .

Mitsoulis, E., S. S. Abdali , and N. C. Markatos, "Flow Simulation of Herschel-Bulkley Fluids Through Extrusion Dies," *Can. J. Chem. Eng.*, **71**, 147 (1993).

Nguyen, Q. D., and D.V. Boger, "Measuring the Flow Properties of Yield Stress Fluids," *Annu. Rev. Fluid Mech.*, **24**, 47 (1992).

O'Donovan, E. J., and R. I. Tanner, "Numerical Study of the Bingham Squeeze Film Problem," *J. Non-Newtonian Fluid Mech.*, **15**, 75 (1984).

Prager, W., *Introduction to Mechanics of Continua,* Ginn, Boston (1961).

Piau, J. M., "Flow of a Yield Stress Fluid in a Long Domain. Application to Flow on an Inclined Plane," *J. Rheol.*, **40**, 711 (1996).

Piau, J. M., *Crucial Elements of Yield Stress Fluid Rheology. Dynamic Complex Fluids,* M. Adams, eds., Royal Society and Imperial Press, London, p. 353 (1998).

Papanastasiou, T. C., "Flow of Material with Yield," *J. of Rheol.,*, **31**, 385 (1987).

Scott, P. S., F. Mirza., and J. Vlachopoulos, "Finite Element Simulation of Laminar Viscoplastic Flows with Region of Recirculation," *J. of Rheol.,* **32**, 387 (1988).

Vradis, G. C., and M. V. Ötügen, "The Axisymmetric Sudden Expansion Flow of a Non-Newtonian Viscoplastic Fluid," *J. Fluid Eng.*, **119**, 193 (1997).

Wilson, S. D. R., "Squeezing Flow of Bingham Material," *J. of Non-Newtonian Fluid Mech.*, **47**, 211 (1993).

Appendix: Pressure and Head Losses

Energy loss between inlet section 1 and exit section 2 can be written as follows:

$$\Delta E_{1,2} = \left\{ P_1 + \rho g z_1 + \frac{1}{2}\rho \frac{U_1^2}{\alpha_1} \right\} - \left\{ P_2 + \rho g z_2 + \frac{1}{2}\rho \frac{U_2^2}{\alpha_2} \right\} \tag{A1}$$

where α_i is a coefficient that depends on the velocity field. For a yield stress fluid, it is possible by integration to obtain

this value:

$$\alpha_i = \frac{\left[a_i^2 + 2a_i(1-a_i)\dfrac{n+1}{2n+1} + (1-a_i)^2\dfrac{n+1}{3n+1}\right]^3}{a_i^2 + 12a_i(1-a_i)\dfrac{(n+1)^3}{(2n+1)(3n+2)(4n+3)} + 3(1-a_i)^2\dfrac{(n+1)^3}{(2n+1)(3n+1)(5n+3)}}, \tag{A2}$$

with

$$a_1 = \frac{\tau_0}{\sigma_{\omega 1}}, \quad a_2 = \frac{\tau_0}{\sigma_{\omega 2}}.$$

For a power-law model $a_1 = a_2 = 0$:

$$\alpha = \frac{(2n+1)(5n+3)}{3(3n+1)^2}. \tag{A3}$$

For a Newtonian model $a_1 = a_2 = 0$, $n = 1$:

$$\alpha = \frac{1}{2}. \tag{A4}$$

The head loss due only to the contraction can be calculated as follows:

$$\Delta E_s = \Delta E_{1,2} - \Delta P_1 - \Delta P_2, \tag{A5}$$

where ΔP_2 and ΔP_1 are the linear pressure drops, respectively, in the inlet and outlet tubes. Pressure drop due to the contraction is also used:

$$\Delta P_S = P_1 - P_2 - \Delta P_1 - \Delta P_2. \tag{A6}$$

If inertia effects are negligible ($Re = 0$), then $\Delta E_s = \Delta P_s$. Usually, ΔP_s and ΔE_s are written as equivalent lengths:

$$L_{\text{eq}} = \frac{\Delta P_s}{2\sigma_{\omega 2}}, \quad L'_{\text{eq}} = \frac{\Delta E_s}{2\sigma_{\omega 2}}. \tag{A7}$$

where L_{eq} is also referred to as the Couette correction.

Manuscript received July 10, 2000, and revision received Dec. 4, 2000.